

In situ 24 kHz coherent imaging of morphology change in laser percussion drilling

Paul J. L. Webster,^{1,*} Joe X. Z. Yu,¹ Ben Y. C. Leung,¹ Mitchell D. Anderson,¹
Victor X. D. Yang,^{2,3,4} and James M. Fraser¹

¹Department of Physics, Engineering Physics and Astronomy, Queen's University, Kingston, Canada K7L 3N6

²Department of Electrical and Computer Engineering, Ryerson University, Toronto, Canada

³Division of Neurosurgery, University of Toronto, Toronto, Canada

⁴Imaging Research, Sunnybrook Health Science Center, Toronto, Canada

*Corresponding author: webster@physics.queensu.ca

Received August 5, 2009; accepted November 13, 2009;
posted January 25, 2010 (Doc. ID 115354); published February 22, 2010

We observe sample morphology changes in real time (24 kHz) during and between percussion drilling pulses by integrating a low-coherence microscope into a laser micromachining platform. Nonuniform cut speed and sidewall evolution in stainless steel are observed to strongly depend on assist gas. Interpulse morphology relaxation such as hole refill is directly imaged, showing dramatic differences in the material removal process dependent on pulse duration/peak power ($\mu\text{s}/0.1\text{ kW}$, $\text{ps}/20\text{ MW}$) and material (steel, lead zirconate titanate PZT). Blind hole depth precision is improved by over 1 order of magnitude using *in situ* feedback from the imaging system. © 2010 Optical Society of America

OCIS codes: 110.4500, 150.5495, 350.3850.

A key challenge in laser micromachining with long duration pulses is overcoming the stochastic damage threshold to achieve reproducible results [1]. Precise material processing is made only more difficult by the subsequent physical state changes, surface chemical reactions, heat and melt flow, and interpulse relaxation and recrystallization. These physical processes have been extensively simulated [2,3], but numerical methods may be reaching their practical limits [4]. Post-cut analysis (e.g., using optical and scanning electron microscopy) has allowed the development of empirical models [5–8] to achieve acceptable results in many applications, but this approach does not overcome inherent stochastic variations. In addition, empirical models are usually correct only for a small range of similar materials and cut parameters, limiting their general applicability. Post-cut analysis cannot directly resolve transient processes occurring during and after laser exposure, which is relevant for understanding the microscopic details of the machining process and pulse-to-pulse accumulation effects. Issues of control are already a concern for processing of homogeneous materials using constant laser repetition rates; high-precision removal will become even more challenging for new composites and highly heterogeneous materials (e.g., tissue), as well as with the introduction of novel process parameters (such as pulse burst machining [9]).

Optical microscopy is a natural fit for *in situ* monitoring of laser machining, with several groups observing the dynamics of depth penetration [10–13]. Coherent microscopy based on variants of optical coherence tomography has been successful at imaging laser-tissue interactions for thermal therapy [14] and surface ablation with 200 Hz frame rates [15]. Overall, these approaches have been limited in applicability owing to specialized light-source requirements, inability to image high-aspect-ratio features, millisecond or slower measurement times, insufficient depth resolution, and/or field of view. The capability

to synchronize the real-time imaging system to the machining laser exposure is also important to truly benefit process development.

In this Letter, we image percussion drilling of industrial materials *in situ* using spectral-domain optical coherence tomography (SD-OCT). SD-OCT axially resolves sample morphology through a Fourier transform of the spectral interferogram resulting from interference between light backscattered from the sample and a reference arm [16]. It exhibits short integration time (8 μs), high sensitivity ($>90\text{ dB}$), high resolution (14 μm), and long field of view ($>1\text{ mm}$) and can image high-aspect-ratio features. Since image acquisition is electronically controlled through the spectrometer camera, image capture is easy to synchronize with the machining laser and microsecond dynamics can be resolved during and after laser exposure. To show its applicability to a wide range of micromachining processes, we compare dynamics in machining with peak irradiances ranging over 5 orders of magnitude using quasi-cw (QCW) and picosecond laser sources. In QCW processing with an industrial Yb-fiber laser, hole refilling between laser pulses is shown to play a significant role in the highly nondeterministic machining process. In addition to easily quantifying machining rates and observing sidewall development in real time (24 kHz), we observe microsecond transients in sample morphology and exploit feedback control to overcome inherent stochastic variations to improve blind hole-depth precision by over 1 order of magnitude.

The custom SD-OCT system is comprised of a broadband $1320\pm 35\text{ nm}$ superluminescent diode light source, a single-mode-fiber 50:50 Michelson interferometer, free-space couplings, and a 24 kHz (maximum) line-rate IR spectrometer. The axial point spread function is 14 μm FWHM in air (dispersion limited). Sensitivity and dynamic range of the system with an 8 μs integration time are measured to be -92 dB and 72 dB , respectively, with 9 mW in-

cident on the sample. Images are processed and displayed logarithmically in M-mode (reflectance versus time and depth) using standard SD-OCT processing: background spectrum subtraction, linear wave number interpolation, fast Fourier transformation, and noise-floor equalization.

The focal volumes of the imaging and cutting beams are overlapped using a dichroic mirror, and the sample is located at their beam waists (machining waist $31\mu\text{m}$ FWHM, imaging waist $35\mu\text{m}$ FWHM). The beam waist for the imaging beam is chosen to simultaneously monitor the primary machining front as well as the volume around the hole. The intense backscatter of the micromachining light does not blind the imaging system, owing to the wavelength filtering of the dichroic mirror and spectrometer. An additional benefit of coherent imaging is that any remaining stray light or $\sim 1300\text{ nm}$ emission from the micromachining process adds only incoherently to the spectral interferogram, isolating its effects to outside the depth of interest.

Machining can be controlled through many parameters, such as pulse energy, duration, and repetition rate. For thermal cutting, the environment can dramatically affect cut rates; for example, the additional thermal power from laser supported oxidation in a high-pressure O_2 environment has been shown to increase material removal [18]. We easily see the detailed dynamics due to O_2 (6.8 bar) for machining of 304 stainless steel (Fig. 1, QCW laser parameters: $100\mu\text{s}$ duration pulses at 4 kHz, center wavelength 1070 nm , 10 mJ [$720\text{ J}/\text{cm}^2$] per pulse on the sample, imaging system synchronized to the middle of the laser pulse). To isolate the contributions specific to high-pressure oxygen, results with no assist gas and N_2 (6.8 bar) are also shown. Interestingly, the counterintuitive result of the machining front retreating with drilling pulse number is sometimes observed. This is attributed to the highly variable interpulse relaxation, as explored in more detail below. Because the optical penetration depth into metal is submicrometer and the imaging spot is larger than the machining beam width, the observed backscatter from depths shallower than the machining front provides information about the sidewalls of the hole being formed, as well as the material surface around the

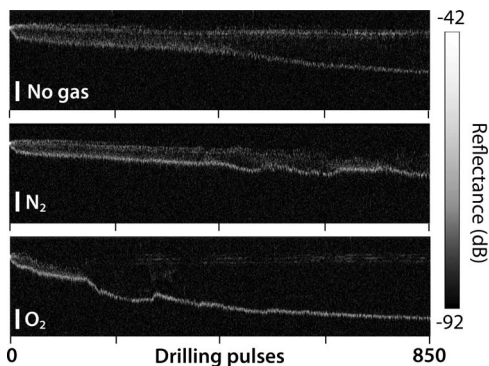


Fig. 1. Hole evolution in QCW drilling of stainless steel, for no gas, N_2 and O_2 assist gases. Light is incident from the top of the figure. Vertical scale bars are $200\mu\text{m}$.

hole. In effect, we access 3D information even with single-axis imaging.

To understand the apparent retreat of the machining front with increasing pulse number, the high-speed and real-time capabilities of the imaging system are essential. Dramatic morphology relaxation between machining pulses is accessed by imaging in bursts slaved to the laser emission [Fig. 2(A); same machining parameters as Fig. 1— O_2 assist gas; six image acquisitions per machining pulse]. The machining front is located to much better than the axial resolution by tracking the centroids of Gaussian fits [Fig. 2(A)i]. Note the clear cycle of material removal and hole refilling (depths over $150\mu\text{m}$). To the best of our knowledge, this is the first real-time observation of this phenomenon in laser micromachining. The depth of hole refilling can be highly variable dependent on the depth penetrated into the sample and is the main cause for the unpredictable behavior in cut speed observed in Fig. 1. In contrast to thermal machining, we also machine the same material through nonlinear optical ablation using a free-space picosecond regenerative amplifier (center wavelength 1064 nm , 10 ps pulse duration, $0.6\text{ TW}/\text{cm}^2$ peak irradiance, 2 kHz repetition rate). Though the total fluence is similar, the much higher peak irradiance induces nonlinear optical ablation with little thermal deposition into the sample [Fig. 2(B)] so that the hole bottom is static between pulses [Fig. 2(B)i]. As expected for nonlinear ablation, the resulting progress of the machining front is highly deterministic.

Interpulse imaging also allows the machining front to be tracked even for the machining of materials with very high removal rates. Figure 2(C) shows processing of lead zirconate titanate (PZT) using only five pulses from the Yb-fiber laser [same QCW drilling parameters as Fig. 2(A)]. The machining rate of PZT is much higher than steel; nearly $750\mu\text{m}$ of material is penetrated after only five drilling pulses. With machining speeds this high, the machining front disappears during laser exposure because of

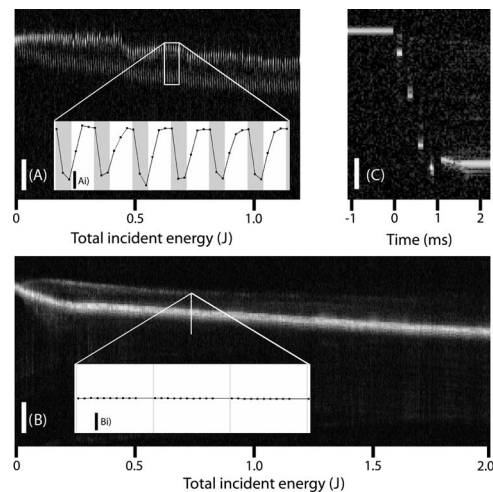


Fig. 2. (A) QCW and (B) picosecond machining in steel; (C) QCW machining in PZT with only five laser pulses. White and black scale bars are $150\mu\text{m}$ and $50\mu\text{m}$, respectively. Gray areas in insets indicate machining laser exposure, and connecting lines are intended as a guide to the eye.

“wash out” of the spectral interferometric fringes [17]. After laser exposure, the front becomes static for the next three axial lines. Note that this loss in contrast, due to motion in SD-OCT, is preferable to the corruption of depth information that can occur in swept-source OCT variants [17].

The high material-removal rates and variable melt flow in QCW drilling limit the precision of blind hole cutting. *In situ* imaging provides the necessary information to allow feedback to correct this problem. We drill eight holes in 304 stainless steel using identical process parameters and image them *ex situ* using the same OCT system with a separate imaging head (XY galvanometer scanning and an 18 mm Thorlabs LSM02 telecentric objective) to capture 3D topography. A side view (additive orthogonal projection) of the holes [Fig. 3(A)] shows a mean depth of 320 μm with a standard deviation of 120 μm . Eight more holes are drilled with the same laser pulse parameters except pulse number. Feedback from the *in situ* imaging system guides the cut to a target depth of 320 μm [Fig. 3(B)]. Standard deviation of the hole depth is reduced by over 1 order of magnitude (to 10 μm) with feedback control. Here, we correct the machining process by manually changing the number of incident pulses; control via other parameters and automatic feedback are also possible.

In summary, we have applied OCT to observe laser machining in industrial materials on microsecond timescales. Since imaging is *in situ* and in real time, we can monitor cut speed and directly optimize common machining parameters (illustrated here with various assist gases). Variations in cut speed in QCW

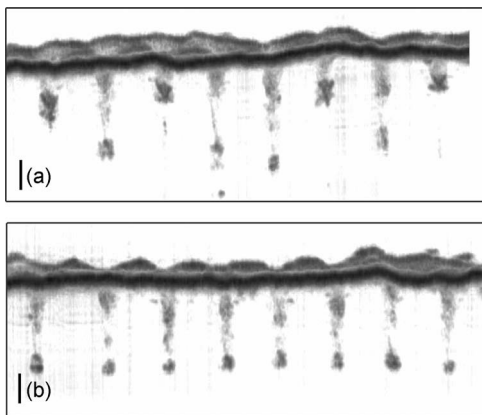


Fig. 3. Side view of 3D surface topography of holes cut (A) without and (B) with feedback (B). Volumes above and below the surface correspond to air and steel, respectively. Scale bars are 100 μm (both axes).

machining are shown to result from highly variable morphology relaxation between laser pulses. Feedback control improves cutting precision as demonstrated for steel, but we anticipate even greater benefits in heterogeneous materials such as laminar composites. Furthermore, the compatibility of OCT and biological imaging (including the ability to image beneath the machining front in materials transparent to IR light) underscores the potential of feedback from this forward-looking imaging capability for guided-laser surgery.

Funding for this work was provided by the Natural Sciences and Engineering Research Council of Canada, the Canadian Foundation for Innovation, Ontario Ministry for Research and Innovation, and the Cancer Imaging Network of Ontario, supported by Cancer Care Ontario.

References

1. A. P. Joglekar, H. Liu, G. J. Spooner, E. Meyhofer, G. Mourou, and A. J. Hunt, *Appl. Phys. B* **77**, 25 (2003).
2. R. K. Ganesh, A. Faghri, and Y. Hahn, *Int. J. Heat Mass Transfer* **40**, 3361 (1997).
3. A. Matsunawa and V. Semak, *J. Phys. D* **30**, 798 (1997).
4. M. S. Gross, I. Black, and W. H. Muller, *Modell. Simul. Mater. Sci. Eng.* **12**, 1237 (2004).
5. I. Black, J. M. Ritchie, and G. A. Thomson, *Lasers Eng.* **7**, 147 (1998).
6. C. H. Li, M. J. Tsai, and C. D. Yang, *Opt. Laser Technol.* **39**, 786 (2007).
7. T. Q. Jia, Z. Z. Xu, X. X. Li, R. X. Li, B. Shuai, and F. L. Zhao, *Appl. Phys. Lett.* **82**, 4382 (2003).
8. U. Zuperl and F. Cus, *Robot. Comput. Integrated Manuf.* **19**, 189 (2003).
9. D. Ilie, C. Mullan, G. M. O'Connor, T. Flaherty and T. J. Glynn, *Appl. Surf. Sci.* **254**, 845 (2007).
10. R. Lausten and P. Balling, *Appl. Phys. Lett.* **79**, 884 (2001).
11. V. V. Temnov, K. Sokolowski-Tinten, P. Zhou, and D. von der Linde, *Appl. Phys. A* **78**, 483 (2004).
12. S. Bera, A. J. Sabbah, C. G. Durfee, and J. A. Squier, *Opt. Lett.* **30**, 373 (2005).
13. P. J. L. Webster, M. S. Muller, and J. M. Fraser, *Opt. Express* **15**, 14967 (2007).
14. B. J. Vakoc, G. J. Tearney, and B. E. Bouma, *J. Biomed. Opt.* **12**, 020501 (2007).
15. W. Y. Oh, S. H. Yun, B. J. Vakoc, G. J. Tearney, and B. E. Bouma, *Appl. Phys. Lett.* **88**, 103902 (2006).
16. A. F. Fercher, W. Drexler, C. K. Hitzenberger, and T. Lasser, *Rep. Prog. Phys.* **66**, 239 (2003).
17. S. H. Yun, G. J. Tearney, J. F. de Boer, and B. E. Bouma, *Opt. Express* **12**, 2977 (2004).
18. W. S. O. Rodden, S. S. Kudesia, D. P. Hand, and J. D. C. Jones, *J. Laser Appl.* **13**, 204 (2001).